Environ. Water Eng., 2025, 11(2), 97-106 DOI: 10.22034/ewe.2024.463604.1943

EWE

Environment and Water Engineering

Homepage: www.jewe.ir

ISSN: 2476-3683

Separation of CO_2 from CH_4 by synthesis hybrid of metal-organic frameworks and covalent-organic frameworks

Mohammad Mehdi Ghasemian[1]✉, Alireza Pardakhti[1], and Mohammad Ali Zahed[2]

[1]Department of Environmental Engineering, Faculty of Environment, University of Tehran, Tehran, Iran
[2]Department of Environment, Faculty of Biological Sciences, Kharazmi University, Tehran, Iran

ARTICLE INFO

Paper Type: Research Paper

Received: 18 June 2024
Revised: 30 July 2024
Accepted: 10 August 2024
Published: 22 May 2025

Keywords
Carbon Dioxide
Methane
Nanocomposite Organic
Metallic Network

***Corresponding author:**
M. M. Ghasemian
✉ mm.ghasemiyan@ut.ac.ir

ABSTRACT

This study synthesized a hybrid COF@MOF nanocomposite combining metal-organic and covalent organic frameworks to enhance CO_2/CH_4 adsorption. An amine-functionalized COF was hydrothermally synthesized to boost selectivity and capacity. Characterization via XRD, SEM, FTIR, and BET analysis confirmed the nanocomposite's structure and high surface area. Adsorption tests under controlled temperature (25–70°C), pressure (0.2–1 bar), and gas concentrations (100 ppm CO_2, 25,000 ppm CH_4) followed a Taguchi L9 orthogonal array. Results revealed pressure-dependent adsorption (direct relationship) and temperature-dependent desorption (inverse relationship), with CO_2 uptake further enhanced by amine-CO_2 acid-base reactions and increased surface area. The process adhered to the Freundlich isotherm, indicating multilayer adsorption. Remarkably, 10 consecutive adsorption-desorption cycles showed <5% efficiency loss, demonstrating exceptional reusability. This work highlights COF@MOF as a high-performance, stable adsorbent for industrial GHG capture, achieving optimized conditions through systematic Taguchi-ANOVA analysis while minimizing experimental runs.

How to cite this paper:
Ghasemian, M. M. , Pardakhti, A., & Zahed, M. A. (2025). Separation of CO_2 from CH_4 by synthesis hybrid of metal-organic frameworks and covalent-organic frameworks. *Environ. Water Eng.*, *11*(2), 97-106. doi: 10.22034/ewe.2024.463604.1943

1. Introduction

The U.S. Energy Information Administration (EIA) has predicted that with the ongoing industrialization of countries, global energy demand will significantly increase by approximately 50% between 2005 and 2030. This substantial growth is particularly evident in the consumption of natural gas, with global consumption of this fossil fuel expected to rise from 95×10^9 ft^3 in 2003 to 182×10^9 ft^3 by 2030 (Lopez-Magano et al., 2020). Methane (CH_4), as the primary constituent of natural gas (comprising about 75 to 90%), plays a key role in this rise in consumption (Li et al., 2024). In addition to CH_4, natural gas contains significant amounts of ethane, propane, butane, and 1 to 3% of other hydrocarbons. The extracted natural gas also contains several pollutants, including carbon dioxide (CO_2), hydrogen sulfide (H_2S), and carbon monoxide (CO), all of which present considerable environmental hazards (Wang et al., 2023). CO_2, due to its acidic properties, is highly corrosive and can rapidly damage pipelines and equipment (Cardoso et al., 2022). Furthermore, CO_2 reduces the calorific value of natural gas flows and causes crystallization during the natural gas liquefaction process (Shen et al., 2023).

The primary factor contributing to the emission of greenhouse gases is the consumption of fossil fuels. CO_2 is one of the significant components in Earth's atmosphere because it absorbs infrared radiation at wavelengths of 4.26 µm and 14.99 µm, leading to the greenhouse effect (Li et al., 2024). This gas is one of the major greenhouse gases that contribute to climate change and global warming (Wang et al., 2023). Controlling CO_2 emissions is a critical issue in managing greenhouse gases. To reduce CO_2 emissions into the atmosphere, three approaches are available: reducing energy consumption, decreasing carbon concentration, and enhancing CO_2 separation (Luo et al., 2022). The concentration of CO_2 in natural gas can vary between 4% and 50%, depending on the

source (Zhu et al., 2024). The goal of CO_2 separation is to capture this gas from sources with suitable concentrations for transportation and utilization. CO_2 separation from gas mixtures is of significant industrial importance. For example, in the production of ammonia and hydrogen from hydrocarbon feedstocks or coal, CO_2 separation from syngas is a crucial step (Wang et al., 2023).

Another application of this technology is in the natural gas purification process, where CO_2 and other acid gases (H_2S and mercaptans) are separated from natural gas. CO_2 separation from CH_4 is significant in various industries, such as natural gas purification and greenhouse gas recycling (Liu et al., 2024).

The adsorption of CO_2 and its separation from CH_4 in porous materials is a highly efficient and effective method for CO_2 capture and sequestration (Mudoi et al., 2022). Today, various gas separation processes have been developed, but surface adsorption technology has gained more importance due to its lower energy consumption, operational simplicity, and distinct applications in industry. In adsorption, a porous solid is used to create a large adsorption surface. The higher the specific surface area and the porosity volume of the adsorbent, the greater its adsorption capacity (Wang et al., 2023; Ma et al., 2017).

Among the porous nanostructured adsorbents that have attracted significant attention for gas adsorption, zeolites (Jin et al., 2023), activated carbon (Chouikhi et al., 2019), carbon nanotubes, mesoporous silica (Toprak et al., 2023), metal-organic frameworks (MOFs), and covalent organic frameworks (COFs) are notable examples (Li et al., 2023; Yang et al., 2022).

Framework materials, including metal-organic frameworks (MOFs) and covalent organic frameworks (COFs), have attracted significant attention due to their widespread applications in various fields such as adsorption (Petit, 2018), catalysis (Bieniek et al., 2021), biomedicine (Yang et al., 2023), and sensing (Zhao et al., 2022). Among these materials, MOFs are particularly notable because they are coordination compounds consisting of organic ligands and metal ions (or clusters), which offer richer properties and more designable structures (Meskher et al., 2023). Unlike zeolites and aluminum phosphates, MOFs stand out as crystalline porous materials, but what differentiates them is their classification as hybrid organic-inorganic compounds rather than purely inorganic ones. At the same time, COFs are introduced as new carbon-based porous nanomaterials with various structures and diverse bonding strengths, either through covalent bonds or weak interactions. The integration of COFs with various functional materials, such as metal oxides, metal nanoparticles, carbon-based materials, silica, quantum dots, and similar substances, opens up the potential for creating novel COF-based composites (Krishnakumar et al., 2022). This integration provides opportunities for developing advanced materials with enhanced properties and capabilities, making COF-based composites a hot topic in research. Overall, both MOFs and COFs continue to contribute significantly to advancements in materials science, offering a broad range of applications and fostering the development of innovative technologies in various fields (Jia et al., 2023).

Novel materials based on MOFs and COFs have garnered significant attention from researchers due to their exceptional capabilities in gas adsorption and separation. MOFs and COFs, with their high specific surface area, tunable porosity, and the possibility of chemical modifications, have been identified as promising materials for gas capture and separation. However, each of these materials has its specific strengths and weaknesses, and combining them in a hybrid form can improve the efficiency and stability of the separation process (Liu et al., 2024). Scientists believe that the solution to environmental challenges may lie in the next generation of MOFs, COFs, and their nanocomposites. In general, the use of nanoscale adsorbents can significantly enhance the efficiency of the gas adsorption process (Wang et al., 2023). MOF@COF nanocomposites, in addition to possessing many of the desirable properties of conventional adsorbents (such as activated carbon), have attracted researchers' interest due to their unique characteristics, such as extremely high surface area, low density, excellent thermal and chemical stability, uniform and size-controlled pores, and high porosity (Sharma and De, 2022).

Given the challenges involved in CO_2 separation from CH_4 and the need for the development of higher-performance materials, research has increasingly focused on the design and synthesis of hybrid MOFs and COFs. These hybrid materials can combine the unique characteristics of both types of materials, offering better performance in gas adsorption and separation. However, studies that comprehensively investigate the performance and mechanisms of these hybrid materials in CO_2 separation from CH_4 are still in the early stages. Therefore, this paper examines and analyzes the synthesis and performance of hybrid MOFs and COFs in CO_2 separation from CH_4 and aims to provide solutions for improving efficiency and reducing the costs associated with this process through the use of these materials.

2. Materials and Methods

For the synthesis of this nanocomposite, MOF-199 was chosen due to its reasonable cost, readily available starting materials, and suitable physical and chemical properties. To enhance the adsorption capacity and selectivity of this MOF, it was composite with amine-functionalized COF. The synthesized adsorbents were characterized using various techniques, including XRD, FT-IR, BET, TGA/DTA, and SEM. The efficiency of these adsorbents in removing CO_2 and CH_4 was evaluated by determining experimental conditions, such as adsorption temperature, adsorption pressure, inlet pollutant gas concentration, and adsorbent mass. The number and conditions of the experiments were based on the initial experimental design. The Langmuir and Freundlich isotherms were used to determine the equilibrium adsorption isotherms. Additionally, experiments were conducted to evaluate the reusability of the adsorbents. To ensure the accuracy of the results, each experiment was repeated three times under similar conditions, and the measurements were recorded.

2.1 Synthesis

2.1.1 Synthesis of MOF

For the synthesis of MOF-199, a hydrothermal method was employed. To begin, 1.76 g of 5,3,1-tricarboxylic acid and 2.85 g of $Cu(NO_3)_2 \cdot 3H_2O$ were dissolved in an equal mixture of 30 ml of ethanol and 30 ml of distilled water. The resulting mixture was stirred for 15 min. Then, the solution was transferred into an autoclave and placed at 80 °C for 24 hr to allow for crystallization. After cooling the mixture to room temperature, the resulting crystals were filtered, washed several times with water and ethanol, and then dried in a conventional oven at 100 °C (Xiang et al., 2010).

2.2 Synthesis of COF@MOF Composite

2.0 g of the MOF synthesized in the previous step was added to a solution prepared by dissolving 5.0 g of melamine and 5.0 g of terephthalaldehyde in 250 ml of dimethyl sulfoxide (DMSO) and 250 ml of distilled water. The resulting solution was placed in an autoclave at 180°C for 12 hr. The final product was filtered, washed with ethanol, and dried at room temperature.

2.3 Adsorption Isotherm Models

For the design of adsorption systems and determination of adsorption characteristics, the Langmuir and Freundlich isotherms were studied. In the Langmuir isotherm, the adsorption of species on the adsorbent occurs homogeneously, meaning that all adsorption sites on the adsorbent are equivalent and the adsorbate forms a monolayer on the surface. In contrast, the Freundlich isotherm represents a heterogeneous adsorption distribution on the adsorbent surface, where different sites have different affinities for the adsorbate, leading to multilayer adsorption. Eq. 1 represents the Langmuir isotherm (Langmuir, 1916):

$$C_e/ q_e = 1/ q_m b + (1/ q_m) C_e \quad (1)$$

where q_e is the adsorption capacity in C_i, mg/g is the initial concentration in C_e, ppm is the final concentration in the solution in V, ppm is the volume of the solution in l, m is the mass of the adsorbent in g, $q_m b$ are Langmuir constants, representing the theoretical maximum monolayer adsorption capacity and the adsorption rate, respectively. The Langmuir isotherm describes adsorption processes where active sites are uniformly distributed on the surface, meaning that the species are adsorbed in a homogeneous, monolayer fashion. The Freundlich isotherm is also an empirical model that describes the adsorption process where the species are adsorbed in a heterogeneous manner on the surface. It is expressed by the following Eq. 2 (Sing, 1998):

$$\ln qe = \ln K_f + (1/n) \ln C_e \quad (2)$$

where K_f and n are the Freundlich constants. From the linear plot of $log(q_{eq})$ versus $log(C_{eq})$, $1/n$ can be determined. The value of $1/n$ indicates the type of isotherm: if $1/n = 0$, the adsorption is irreversible; if $1<1/n<0$, the adsorption is favorable; and if $1/n>1$, the adsorption is unfavorable.

2.4 COF@MOF Adsorbent Bed System for Adsorption of CO_2 and CH_4 Gases

The adsorption system consists of a horizontally simulated column resembling a chimney, where sampling points are incorporated at various locations to measure the velocity, pressure, temperature, and concentration of the incoming and outgoing gases from the adsorbent. The CH_4 and CO_2 gases are introduced into the system through calibrated reference cylinders. After calibration, the instrumentation equipment is installed at specific points to measure the velocity, temperature, humidity, and gas concentration. A schematic of the gas adsorption process is shown in Fig. 1. In this experiment, a defined amount of adsorbent bed is exposed to a specific concentration of CH_4 and CO_2 gases. The concentrations of these gases are measured simultaneously before entering and after exiting the bed. Then, the varying adsorption parameters such as temperature, pressure, and the mass of the adsorbent are investigated under different conditions.

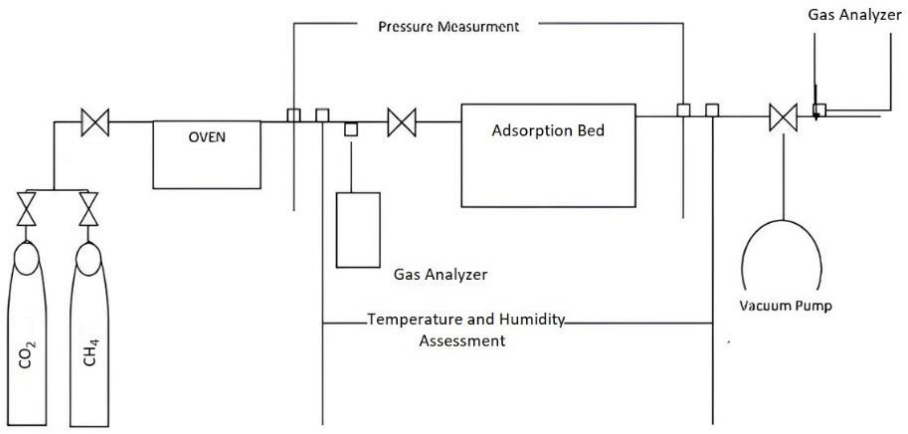

Fig. 1 Schematic of gas adsorption instrument

Before the experiment, preliminary operations were carried out, including the calibration of all equipment, such as the pressure gauge, flow meter, air compressor performance test, hydro-testing of equipment and connections, loading the adsorbent bed, adjusting the compressor pressure, and testing the gas analyzers. Initially, the air was passed through the system for a while to allow the temperature and humidity on both sides of the column to reach equilibrium. During this process, ensuring the system's leak-tightness was essential. To ensure this, ceramic wool was used in the sections where the equipment was installed. After completing these preparations, the concentrations of CH_4 and CO_2 gases were measured at specified time intervals (every 90 s) before and after passing

through the adsorbent, and all varying parameters were analyzed. Finally, the adsorption isotherms were also plotted.

Before the experiment, preliminary operations were conducted, including calibrating all equipment (e.g., pressure gauge, flow meter), testing the air compressor's performance, performing hydro-tests on equipment and connections, loading the adsorbent bed, adjusting the compressor pressure, and verifying the gas analyzers. Initially, air was passed through the system to allow temperature and humidity equilibration on both sides of the column. Throughout this process, ensuring system leak-tightness was critical. Ceramic wool was used to seal sections where equipment was installed. The efficiency of the synthesized adsorbent in removing CO_2 and CH_4 was evaluated under controlled experimental conditions, including adsorption temperature, pressure, and inlet pollutant gas concentrations. The number and conditions of the experiments followed the initial design (Table 1). Tests were repeated for different adsorbent masses, target pressures, and temperatures, with results recorded at each stage.

Table 1 Design of the experiment using the Taguchi method

Run	Factor 1 Pressure (bar)	Factor 2 Temperature (ºC)	Factor 3 CH_4 (ppm)	Factor 4 CO_2 (ppm)
1	0.2	25	25000	100
2	0.8	25	25000	100
3	1	25	25000	100
4	0.2	50	25000	100
5	0.8	50	25000	100
6	1	50	25000	100
7	0.2	70	25000	100
8	0.8	70	25000	100
9	1	70	25000	100

Various instruments and equipment were used in these experiments to ensure accurate and reliable results. The adsorption reactor, the system's core component, was made of stainless steel with precise dimensions. Designed to withstand high pressures, it enabled controlled adsorbent placement.

A high-performance vacuum pump generated the necessary low-pressure conditions for complete gas desorption. Gas concentrations at the reactor inlet and outlet were measured using advanced gas analyzers, including Gas Chromatography (GC) and Fourier Transform Infrared Spectroscopy (FTIR), ensuring high-precision monitoring over time. Temperature and pressure were precisely regulated using advanced controllers, maintaining ranges of 0–70°C and 0–1 bar, respectively. A data logger recorded measurements continuously, minimizing human error and enabling reliable data storage. All equipment was calibrated before use to guarantee measurement accuracy throughout the experiments.

After each adsorption and desorption cycle, data were collected through both quantitative and qualitative measurements. The adsorbed gas quantity was calculated based on the difference between inlet and outlet gas concentrations. High-precision gas analyzers—including GC and FTIR—were employed to measure CO_2 and CH_4 concentrations. The recorded parameters included: temperature and pressure, inlet and outlet gas concentrations, time required to reach equilibrium, and number of repeated adsorption/desorption cycles. The equilibrium time was specifically documented for each experimental run to assess kinetic performance.

The efficiency of the adsorbent was calculated using Eq. 1:

$$\eta = \frac{C_{in} - C_{out}}{C_{in}} \times 100 \quad (1)$$

where: η: adsorption efficiency (%), C_{in}: initial concentration of pollutant gas (ppm), and C_{out}: outlet concentration of pollutant gas (ppm).

Adsorption capacity was defined as the amount of gas adsorbed per unit mass of the adsorbent and was calculated using Eq. 2:

$$q = \frac{(C_{in} - C_{out}) \times V}{m} \quad (2)$$

where: q: adsorption capacity (mg/g), V: Volume of gas passed (l), and m: Mass of the adsorbent (g).

The Taguchi experimental design method was used to optimize the experimental conditions. The purpose of this optimization was to determine the optimal conditions for maximum gas adsorption. After conducting the experiments, the data were entered into statistical analysis software, and the results were reported in the form of variable impact graphs and condition optimization.

To ensure the accuracy and reliability of the results, each experiment was repeated at least three times. Additionally, to evaluate reproducibility and data accuracy, the results obtained from different repetitions were compared, and the standard deviation was calculated. Acceptable reproducibility is achieved when the standard deviation of the results is less than

5%.To investigate the effect of various variables (pressure, temperature, CO_2 concentration, and CH_4 concentration) on adsorption efficiency, Analysis of Variance (ANOVA) was used. This analysis made it possible to identify the most influential variables and determine their optimal levels. Additionally, the results were graphically analyzed using statistical analysis software.

2.5 Experiments

The experiments were designed using the Taguchi method with an L9 orthogonal array, incorporating four controlled factors: Pressure (0.2, 0.8, 1 bar), Temperature (25, 50, 70°C), CH_4 concentration (constant at 25,000 ppm), and CO_2 concentration (constant at 100 ppm). Nine experimental runs were conducted, each representing a unique combination of these factors. To assess experimental error and statistical reliability, the central point (Run 2) was replicated three times. This methodology significantly reduced the experimental workload while enabling robust optimization of the adsorption process.

Data analysis was performed using Analysis of Variance (ANOVA) to identify the most influential factors and their optimal levels. The results revealed key insights into the impact of each parameter on adsorption efficiency, facilitating systematic optimization of process conditions.

3. Results and Discussion

3.1 Characterization of synthesized nanoadsorbent

3.1.1 X-ray diffraction analysis

To examine the pore structure of the synthesized compounds, X-ray Diffraction (XRD) patterns were obtained for the synthesized MOF and MOF@COF adsorbents (Fig. 2). The XRD pattern of the MOF sample shows the main peaks at 2θ positions of 9.4°, 11.62°, 17.4°, 19°, and 23.3° with relative intensities corresponding to those previously reported, confirming the formation of this metal-organic framework (Thi et al., 2013). According to Fig. 2, the primary structure remained intact after composite formation, and the original structure was preserved. The intensity of the peaks in MOF@COF, especially the main peak, slightly decreased, which could be attributed to the incorporation of the functional groups from COF into the MOF structure.

By examining Fig. 2, it can be observed that the original structure of MOF remains intact after being combined with COF and is well preserved. However, the intensity of the peaks (especially the main peak) in the MOF@COF sample has decreased. This reduction in intensity could be attributed to the incorporation of COF functional groups into the MOF structure. This suggests that during the composite formation process, COF groups have been integrated into the MOF structure, resulting in changes in X-ray diffraction patterns and consequently a decrease in peak intensity. Overall, these results indicate that the original MOF structure is maintained even after combining with COF, although some changes in peak intensity are observed due to the influence of COF.

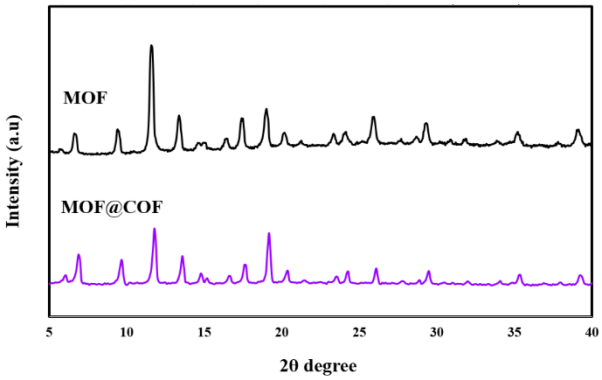

Fig. 2 XRD pattern of the adsorbents synthesized

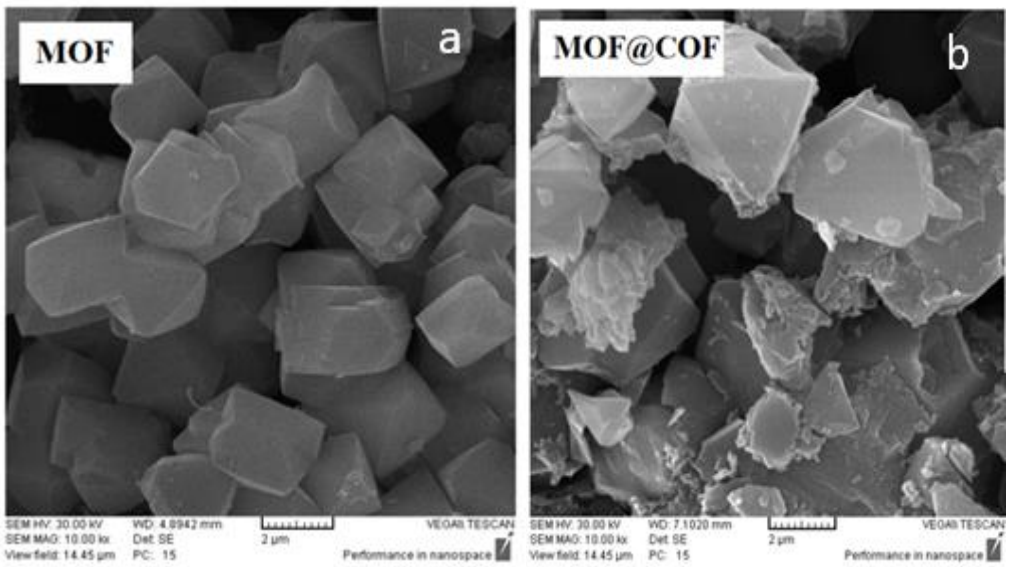

Fig. 3 SEM images of the adsorbents synthesized a) MOF, b) MOF@COF

3.1.2 Scanning Electron Microscopy (SEM) Images

SEM images were used to demonstrate the morphology of the synthesized adsorbents. Fig. 3 shows the SEM images of the MOF network before and after composite formation. As observed, the image corresponding to MOF displays pyramid-shaped crystals with sharp edges and particle sizes of

approximately 10 µm. This image effectively illustrates the purity of the synthesized compound, as no needle-shaped particles, which would indicate unreacted ligands, are visible (Xie et al., 2012). The images of the MOF@COF composite indicate that the MOF structure synthesized did not undergo any significant changes after composite formation, and its structure was preserved before and after the compositing process.

3.1.3 Nitrogen Adsorption-Desorption Analysis

Fig. 4 shows the adsorption and desorption isotherms of nitrogen for the synthesized adsorbents. The gas adsorption isotherm is of type IV, which aligns with the IUPAC classification for mesoporous materials (Buttersack, 2019). Additionally, the isotherm shows a hysteresis loop, indicating that the adsorbents are mesoporous (Jun et al., 2000). Using the BET method, the specific surface area, pore size, and pore volume were measured.

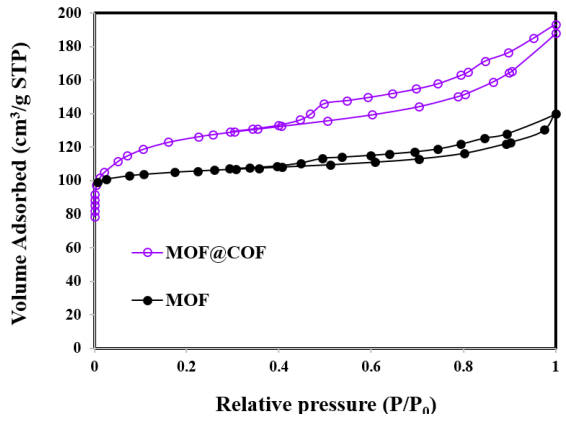

Fig. 4 BET isotherms of the adsorbents synthesized

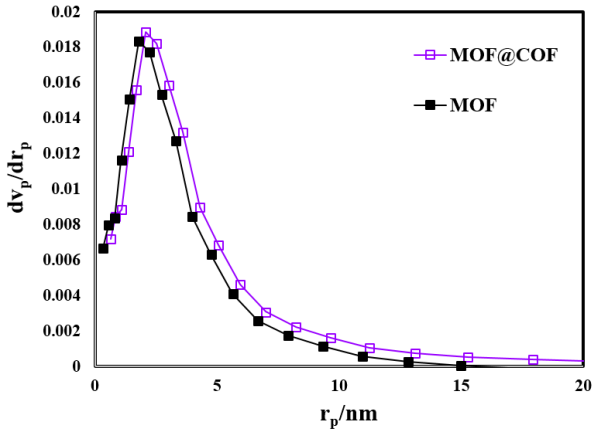

Fig. 5 Pore size distribution of the adsorbents synthesized

The pore size distribution was obtained using the Barrett-Joyner-Halenda method (Fig. 5). The results for MOF and MOF@COF show a uniform pore size distribution with values around 2.15 and 2.35 nm, indicating mesopores within the range. These results further confirm the structure of the synthesized compounds, which possess mesoporous cavities (Horvat et al., 2022).

3.1.4 FT-IR Spectroscopic Analysis

The FT-IR spectrum of the synthesized adsorbents is shown in Fig. 6. The comparison of the FT-IR spectrum with previous studies for the MOF compound confirms the successful synthesis of this compound (Garg et al., 2022). The presence of sharp, high-intensity bands in the range of 1450-1650 cm^{-1} corresponds to the stretching vibrations of the C-C bond in the aromatic ring. A weak C-H aromatic ring stretching band at 3050 cm^{-1} further confirms this (Maurya et al., 2016). The presence of the aromatic ring indicates that the organic ligand used in the final structure of the adsorbent remains intact and has not decomposed. The peak in the range of 1540-1630 cm^{-1} represents the stretching vibrations of the C-O group, while the broadband in the range of 2500-3500 cm^{-1} is attributed to the OH vibrations from water and ethanol molecules present in the compound (Yadav et al., 2021). In MOF@COF, the peaks at 1410, 1230, and 550 cm^{-1} can be attributed to the stretching vibrations of C-N in the secondary amine, in-plane C-H aromatic vibrations, and out-of-plane C-H vibrations, respectively. NH-related vibrations appear in the range of 1460-1560 cm^{-1} (Mekoung et al., 2022).

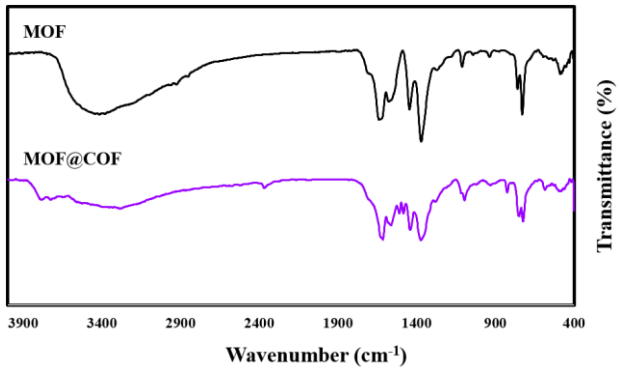

Fig. 6 FTIR spectra of the adsorbents synthesized

3.1.5 Thermal Stability Analysis (TGA/DTA)

Fig. 7 shows that the weight loss of MOF increases with temperature in two stages. The first stage, with weight loss at temperatures below 110 °C, is mainly due to the loss of surface and internal water from the sample. During this stage, a 15% weight reduction was observed. The second stage, a 25% weight loss between 180 °C and 250 °C, is related to the degradation of OH groups and the decomposition of the organic framework of the compound. According to the results from the TGA, the MOF structure is degraded at temperatures above 250 °C, so that at 650°C it transforms into its stable oxide form, likely converting into copper oxide. The TGA curve of this compound confirms the relatively low stability of the MOF due to the presence of organic components in its structural framework (An et al., 2024). After adding COF to the MOF network structure, the results show that MOF@COF exhibits greater thermal stability compared with MOF, indicating that this synthesized hybrid nanocomposite has relatively good stability.

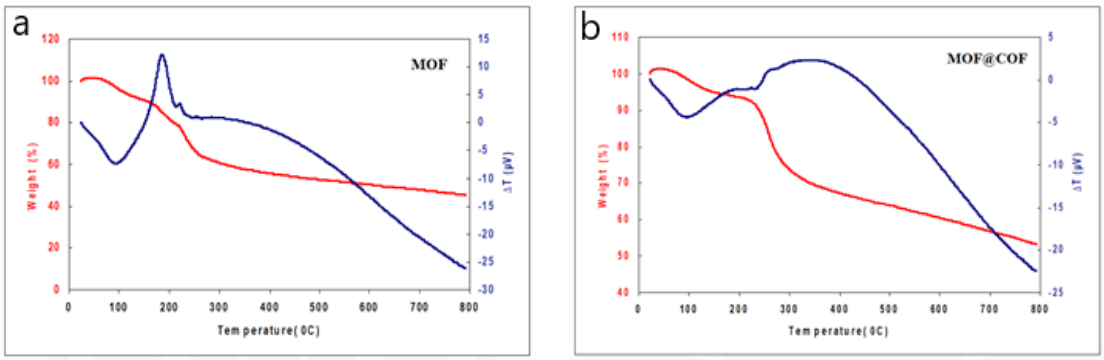

Fig. 7 TGA thermograms of the adsorbents synthesized a) MOF, and b) MOF@COF

3.2 Adsorption Experiments

3.2.1 Results of CO_2 and CH_4 Adsorption Experiments

The amount of gas adsorbed by the adsorbent at each stage of the process is determined by calculating the molar balance between the initial and final thermodynamic states of the gas phase in the system, using an appropriate equation of state. To determine the total amount of gas adsorbed during the process, the amount of gas adsorbed at each stage is added to the sum of the gas adsorbed in all previous stages. In the initial state, before the adsorption process begins and with the adsorption bed valve closed, the gas in the reference column and its connections are at different pressure conditions than the gas in the adsorption tank containing the adsorbent. This pressure difference between the gas phases before and after adsorption forms the basis for calculating the amount of adsorption at each stage. By performing these calculations at each stage and summing them up, the total amount of gas adsorbed by the adsorbent throughout the process can be precisely determined. In the secondary state, after the adsorption process is completed, the connection between the adsorption column and the rest of the system is established, and the gas throughout the system reaches a uniform pressure equilibrium. This equilibrium state indicates the end of the adsorption process at that stage. The results from experiments conducted under various temperature and pressure conditions on adsorption with the adsorbent are presented in Table 2. This table shows the effect of temperature and pressure on the amount of gas adsorbed by the adsorbent. It can serve as a basis for analyzing the performance of the adsorbent.

Table 2 Effect of temperature and pressure changes on adsorption of CO_2 and CH_4 using MOF@COF

Adsorbent dosage (g)	Pressure (ba)	Temperature °C	CO_2 concentration (ppm)		CH_4 concentration (ppm)	
			Before adsorption	After adsorption	Before adsorption	After adsorption
100	0.2	25	10	10	25000	2091
100	0.2	50	10	18	25000	2416
100	0.2	70	10	24	25000	2918
Pressure changes						
100	25	0.2	10	11	25000	2100
100	25	0.8	10	9	25000	1920
100	25	1	10	6	25000	1800

The best conditions were observed at a temperature of 25°C and a pressure of 1 bar. As the temperature increased, the adsorption efficiency decreased, while an increase in pressure resulted in a direct increase in adsorption. The regeneration of the adsorbent refers to its ability to function effectively for multiple cycles of contact with the adsorbate species. The highest adsorption capacity occurs during the first contact with the adsorbate, as the greatest number of active sites are involved in the adsorption process at this stage. In subsequent contacts, some adsorption sites may either separate from the adsorbent or remain occupied. Adsorbents with repeatable adsorption capacities are considered suitable and economically viable.

To evaluate the reusability of the synthesized nanocomposite, adsorption and desorption processes were carried out over 10 cycles. The results showed that the performance of the COF@MOF nanocomposite remained stable with negligible change across the 10 adsorption-desorption cycles. According to desorption results, the adsorbent showed a 33% reduction in CO_2 adsorption efficiency (from 100 to 9 ppm) and an 18% decrease in CH_4 adsorption efficiency (from 2500 to 2186 ppm) after 10 cycles, indicating the efficiency of the hybrid adsorbent.

3.2.2 Adsorption isotherms

The Langmuir and Freundlich adsorption isotherm constants were calculated using Eqs. 1 and 2, and the results are reported in Table 3. Considering the value of R^2, which indicates the degree of linearity and the correlation of the curve obtained from plotting the adsorption isotherm diagrams, it can be concluded that the adsorption mechanism of the targeted gases is more consistent with the Freundlich isotherm.

Table 3 Calculated constants of Langmuir and Freundlich isotherms

Pollutant	Langmuir isotherm			Freundlich isotherm		
	q_m	b	R^2	K_F	n	R^2
CO_2	68.96	0.0132	0.8098	6.730	0.235	0.9900
CH_4	73.52	0.0133	0.9531	159.62	0.139	0.9992

4. Conclusion

In this study, a hybrid nanocomposite composed of MOF and COF was synthesized for the removal of CO_2 and CH_4, due to its unique physical and chemical properties. To enhance the adsorption capacity and improve the selectivity of this nanocomposite, amino-functionalized COF, synthesized via the hydrothermal method, was utilized. The synthesized nanocomposite (COF@MOF) was identified and characterized using various techniques, including XRD, SEM, FTIR, and BET. The performance of the COF@MOF nanocomposite in removing CO_2 and CH_4 under different experimental conditions, such as temperature, pressure, and the concentration of incoming pollutant gases, was evaluated using an initial experimental design method based on the Taguchi approach. This experimental design method helped optimize the conditions and identify the parameters affecting the performance of the adsorbent. The results showed that:

1. The amount of adsorption had a direct relationship with pressure and an inverse relationship with temperature. Specifically, the adsorption efficiency increased with pressure and decreased with temperature.

2. According to the R^2 value, the adsorption mechanism of CO_2 and CH_4 in the synthesized nanocomposite follows the Freundlich isotherm.

3. The performance of the COF@MOF nanocomposite did not significantly change over the 10 cycles of adsorption and desorption.

While the COF@MOF nanocomposite maintained its performance after 10 adsorption-desorption cycles, long-term stability over hundreds or thousands of cycles must be evaluated for industrial feasibility. Additionally, its performance in removing other industrial gases remains unexplored. Laboratory conditions differ from real-world industrial environments, where variations in temperature, pressure, and humidity may impact efficiency. Moreover, the production cost and scalability of the synthesis process have not been assessed, which are crucial for industrial adoption. Future research should focus on extending adsorption-desorption cycle testing, examining the impact of diverse gas mixtures, and evaluating performance under actual industrial conditions. Economic feasibility and scalability assessments are essential for practical implementation. Additionally, exploring new hybrid nanocomposites with enhanced properties could lead to superior adsorbents for broader applications.

Statements and Declarations

Data availability

The data used in this research are provided in the text of the article.

Conflicts of interest

The author of this paper declared no conflict of interest regarding the authorship or publication of this paper.

Author contribution

M.M. Ghasemian: Modeling and Results Analysis; A. Pardakhti: Research Management and M.A. Zahed: Data Collection.

AI Use Disclosure

During the preparation of this manuscript, the authors used ChatGPT for language translation. All content has been carefully reviewed and revised by the authors, who take full responsibility for the final version of the manuscript.

References

An, Y., Lv, X., Jiang, W., Wang, L., Shi, Y., Hang, X., & Pang, H. (2024). The stability of MOFs in aqueous solutions—Research progress and prospects. *Green Chem. Eng.*, *5*(2), 187–204. DOI: 10.1016/j.gce.2023.07.004

Bieniek, A., Terzyk, A. P., Wiśniewski, M., Roszek, K., Kowalczyk, P., Sarkisov, L., Keşkin, S., & Kaneko, K. (2021). MOF materials as therapeutic agents, drug carriers, imaging agents and biosensors in cancer biomedicine: Recent advances and perspectives. *Prog. Mater. Sci.*, *117*, 100743. DOI: 10.1016/j.pmatsci.2020.100743

Buttersack, S. (2019). Modeling of type IV and V sigmoidal adsorption isotherms. *Phys. Chem. Chem. Phys.*, *21*(10), 5614–5626. DOI: 10.1039/C8CP07751G

Cardoso, A. R. T., Ambrosi, A., Di Luccio, M., & Hotza, D. (2022). Membranes for separation of CO_2/CH_4 at harsh conditions. *J. Nat. Gas Sci. Eng.*, *98*, 104388. DOI: 10.1016/j.jngse.2021.104388

Chouikhi, N., Cecilia, J. A., Vilarrasa-García, E., Besghaier, S., Chlendi, M., Franco Duro, F. I., Castellon, E. R., & Bagane, M. (2019). CO_2 adsorption of materials synthesized from clay minerals: A review. *Miner.*, *9*(9), 514. DOI: 10.3390/min9090514

Garg, D., Rekhi, H., Kaur, H., Singh, K., & Malik, A. K. (2022). A novel method for the synthesis of MOF-199 for sensing and photocatalytic applications. *J. Fluor.*, *32*(3), 1171–1188. DOI: 10.1007/s10895-022-02902-9

Horvat, G., Pantić, M., Knez, Z., & Novak, Z. (2022). A brief evaluation of pore structure determination for bioaerogels. *Gel.*, *8*(7), 438. DOI: 10.3390/gels8070438

Jia, P., He, X., Yang, J., Sun, X., Bu, T., Zhuang, Y., & Wang, L. (2023). Dual–emission MOF–based ratiometric platform and sensory hydrogel for visible detection of biogenic amines in food spoilage. *Sens. Actuat. B: Chem*., *374*, 132803. DOI: 10.1016/j.snb.2022.132803

Jin, Y., Xu, Q., Zheng, F., & Lu, J. (2023). Enhancement in CO_2 adsorption by zeolite synthesized from co-combustion ash of coal and rice husk modified with lithium ion. *J. Energy Inst.*, *110*, 101348. DOI: 10.1016/j.joei.2023.101348

Jun, S., Joo, S. H., Ryoo, R., Kruk, M., Jaroniec, M., Liu, Z., Ohsuna, T., & Terasaki, O. (2000). Synthesis of new, nanoporous carbon with hexagonally ordered mesostructure. *J. Am. Chem. Soc.*, *122*(43), 10712–10713. DOI: 10.1021/ja002261e

Krishnakumar, A., Mishra, R. K., Kadian, S., Zareei, A., Rivera, U. H., & Rahimi, R. (2022). Printed graphene-based electrochemical sensor with integrated paper microfluidics for rapid lidocaine detection in blood. *Analyt. Chim. Acta*, *1229*, 340332. DOI: 10.1016/j.aca.2022.340332

Langmuir, I. (1916). The constitution and fundamental properties of solids and liquids. Part I. Solids. *J. Am. Chem. Soc*., *38*(11), 2221–2295. DOI: 10.1021/ja02268a002

Li, G., Kujawa, J., Knozowska, K., Kareiva, A., Favre, E., Castel, C., & Kujawski, W. (2024). The advancements in mixed matrix membranes containing functionalized MOFs and 2D materials for CO_2/N_2 separation and CO_2/CH_4 separation. *Carbon Capt. Sci. Technol*., *13*, 100267. DOI: 10.1016/j.ccst.2023.100267

Li, G., Wang, M., Zhou, W., Liu, X., Zhu, Z., Song, X., & Huo, P. (2023). Fabricating MOF@COF core–shell catalyst with remarkable CO_2 adsorption capacity and charge carrier dynamics for efficient CO_2 conversion. *J. Alloy. Compound*., *968*, 171919. DOI: 10.1016/j.jallcom.2023.171919

Liu, Y., Li, P., Cui, R., Qin, C., Wu, L., Zhang, X., Li, B., Ping, J., Wang, Y., Pan, J., Ying, Y., Li, D., Shi, D., & Xu, L. (2024). Metal–organic frameworks (MOFs) and covalent organic frameworks (COFs)–based prototyping of integrated sensing devices for robust analysis. *Trend. Anal. Chem*., *117678*. DOI: 10.1016/j.trac.2024.117678

Lopez-Magano, A., Jimenez-Almarza, A., Aleman, J., & Mas-Balleste, R. (2020). Metal–organic frameworks (MOFs) and covalent organic frameworks (COFs) applied to photocatalytic organic transformations. *Catal.*, *10*(7), 720. DOI: 10.3390/catal10070720

Luo, W., Niu, Z., Mu, P., & Li, J. (2022). MXene/poly(ethylene glycol) mixed matrix membranes with excellent permeance for highly efficient separation of CO_2/N_2 and CO_2/CH_4. *Colloid. Surf. A: Physicochem. Eng. Aspect*., *640*, 128481. DOI: 10.1016/j.colsurfa.2022.128481

Ma, Y., Wang, Z., Xu, X., & Wang, J. (2017). Review on porous nanomaterials for adsorption and photocatalytic conversion of CO_2. *Chin. J. Catal*., *38*(12), 1956–1969. DOI: 10.1016/S1872-2067(17)62955-3

Maurya, A., Rastogi, S., Rouillé, G., Huisken, F., & Henning, T. (2012). Experimental and theoretical study on the infrared spectroscopy of astrophysically relevant polycyclic aromatic hydrocarbon derivatives 2- and 9-vinylanthracene. *Astrophys. J*., *755*(2), 120. DOI: 10.1088/0004-637X/755/2/120

Mekoung, P. M. A., Mountessou, B. Y. G., Mbah, M. B., Signe, M., Zintchem, A. A. A., Nanseu, C. P. N., & Mbouombouo, I. N. (2022). Vibrational spectroscopic investigations, electronic properties, molecular structure and quantum mechanical study of an antifolate drug: pyrimethamine. *Comput. Chem*., *10*(4), 157–185. DOI: 10.4236/cc.2022.104008

Meskher, H., Belhaouari, S. B., & Sharifianjazi, F. (2023). Mini review about metal–organic framework (MOF)–based wearable sensors: Challenges and prospects. *Heliyon*, *9*(11), e21621. DOI: 10.1016/j.heliyon.2023.e21621

Mudoi, M. P., Sharma, P., & Khichi, A. S. (2022). A review of gas adsorption on shale and the influencing factors of CH_4 and CO_2 adsorption. *J. Petrol. Sci. Eng*., *217*, 110897. DOI: 10.1016/j.petrol.2022.110897

Petit, C. (2018). Present and future of MOF research in the field of adsorption and molecular separation. *Current Opinion Chem. Eng*., *20*, 132–142. DOI: 10.1016/j.coche.2018.04.004

Sharma, V., & De, D. (2021). CO_2 adsorption with covalent organic framework (COF). In *Nanomaterials for CO_2 Capture, Storage, Conversion and Utilization* (pp. 53–86). Elsevier. DOI: 10.1016/B978-0-12-822894-4.00005-8

Shen, J., Wang, X., & Chen, Y. (2023). Adsorbents for adsorption separation of CO_2 and CH_4: A literature review. *Canad. J. Chem. Eng*., *101*(12), 7115–7133. DOI: 10.1002/cjce.24942

Sing, K. S. (1998). Adsorption methods for the characterization of porous materials. *Adv. Colloid. Inter. Sci*., *76*, 3–11. DOI: 10.1016/S0001-8686(98)00038-4

Thi, T. V. N., Luu, C. L., Hoang, T. C., Nguyen, T., Bui, T. H., Nguyen, P. H. D., & Thi, T. P. P. (2013). Synthesis of MOF-199 and application to CO_2 adsorption. *Adv. Nat. Sci.: Nanosci. Nanotechnol.*, *4*(3), 035016. DOI: 10.1088/2043-6262/4/3/035016

Toprak, A., & Hazer, B. (2023). Synthesis of microporous hollow spherical polystyrene carbons for the highly

efficient CO_2 adsorption and selectivity. *J. Indust. Eng. Chem*., *127*, 295–302. DOI: 10.1016/j.jiec.2023.07.015

Wang, S., Zhou, S., Pan, Z., Elsworth, D., Yan, D., Wang, H., Liu, D., & Hu, Z. (2023). Response of pore network fractal dimensions and gas adsorption capacities of shales exposed to supercritical CO_2: Implications for CH_4 recovery and carbon sequestration. *Energy Reports*, *9*, 6461–6485. DOI: 10.1016/j.egyr.2023.05.266

Xiang, Z., Cao, D., Shao, X., Wang, W., Zhang, J., & Wu, W. (2010). Facile preparation of high-capacity hydrogen storage metal–organic frameworks: A combination of microwave-assisted solvothermal synthesis and supercritical activation. *Chem. Eng. Sci*., *65*(10), 3140–3146. DOI: 10.1016/j.ces.2010.02.005

Xie, J., Yan, N., Qu, Z., & Yang, S. (2012). Synthesis, characterization and experimental investigation of Cu-BTC as CO_2 adsorbent from flue gas. *J. Environ. Sci*., *24*(4), 640–644. DOI: 10.1016/S1001-0742(11)60841-3

Yadav, A., Moharrami, N., & Bull, S. (2021). Investigation of chemomechanical effects on sapphire surfaces modified by ion-implantation-induced carbon impurities. *J. Bio- and Tribo-Corr*., *7*, 52. DOI: 10.1007/s40735-021-00490-y

Yang, Y., Jin, L., Zhou, L., & Du, X. (2022). A molecular study of humid CO_2 adsorption capacity by Mg-MOF-74 surfaces with ligand functionalization. *Comput. Mater. Sci*., *209*, 111407. DOI: 10.1016/j.commatsci.2022.111407

Yang, Z. W., Li, J. J., Wang, Y. H., Gao, F. H., Su, J. L., Liu, Y., Wang, Y. H., & Ding, Y. (2023). Metal/covalent-organic framework-based biosensors for nucleic acid detection. *Coordinat. Chem. Rev*., *491*, 215249. DOI: 10.1016/j.ccr.2023.215249

Zhao, L., Song, X., Wang, H., Wang, X., Wu, D., Wei, Q., & Ju, H. (2022). Eu(II)-MOF as NIR probe for highly efficient instantaneous anodic electroluminescence realized environmental pollutant trace monitoring. *Chem. Eng. J*., *446*, 136912. DOI: 10.1016/j.cej.2022.136912

Zhu, W., Chen, M., Jang, J., Han, M., Moon, Y., Kim, J., You, J., Li, S., Park, T., & Kim, J. (2024). Amino-functionalized nanocellulose aerogels for the superior adsorption of CO_2 and separation of CO_2/CH_4 mixture gas. *Carbohyd. Polymer*., *323*, 121393. DOI: 10.1016/j.carbpol.2023.121393